

Article

Lignin–Chitosan Nanocarriers for the Delivery of Bioactive Natural Products against Wood-Decay Phytopathogens

Eva Sánchez-Hernández ¹, Natalia Langa-Lomba ^{2,3}, Vicente González-García ³, José Casanova-Gascón ², Jesús Martín-Gil ^{1,*}, Alberto Santiago-Aliste ¹, Sergio Torres-Sánchez ⁴ and Pablo Martín-Ramos ²

¹ Department of Agricultural and Forestry Engineering, ETSIIAA, University of Valladolid, Avenida de Madrid 44, 34004 Palencia, Spain; eva.sanchez.hernandez@uva.es (E.S.-H.); alberto.santiago@alumnos.uva.es (A.S.-A.)

² Instituto Universitario de Investigación en Ciencias Ambientales de Aragón (IUCA), EPS, University of Zaragoza, Carretera de Cuarte s/n, 22071 Huesca, Spain; natalialangalomba@gmail.com (N.L.-L.); jcasan@unizar.es (J.C.-G.); pmr@unizar.es (P.M.-R.)

³ Plant Protection Unit, Instituto Agroalimentario de Aragón-IA2 (CITA-Universidad de Zaragoza), Avda. Montañana 930, 50059 Zaragoza, Spain; vgonzalezg@aragon.es

⁴ Viñas del Vero S.A., Carretera Nacional 123 (km 3.7), 22300 Barbastro, Spain; storres@vinasdelvero.es

* Correspondence: mgil@iaf.uva.es; Tel.: +34-(979)-108347

Abstract: The use of nanocarriers (NCs), i.e., nanomaterials capable of encapsulating drugs and releasing them selectively, is an emerging field in agriculture. In this study, the synthesis, characterization, and in vitro and in vivo testing of biodegradable NCs loaded with natural bioactive products was investigated for the control of certain phytopathogens responsible for wood degradation. In particular, NCs based on methacrylated lignin and chitosan oligomers, loaded with extracts from *Rubia tinctorum*, *Silybum marianum*, *Equisetum arvense*, and *Urtica dioica*, were first assayed in vitro against *Neofusicoccum parvum*, an aggressive fungus that causes cankers and diebacks in numerous woody hosts around the world. The in vitro antimicrobial activity of the most effective treatment was further explored against another fungal pathogen and two bacteria related to trunk diseases: *Diplodia seriata*, *Xylophilus ampelinus*, and *Pseudomonas syringae* pv. *syringae*, respectively. Subsequently, it was evaluated in field conditions, in which it was applied by endotherapy for the control of grapevine trunk diseases. In the in vitro mycelial growth inhibition tests, the NCs loaded with *R. tinctorum* resulted in EC₉₀ concentrations of 65.8 and 91.0 µg·mL⁻¹ against *N. parvum* and *D. seriata*, respectively. Concerning their antibacterial activity, a minimum inhibitory concentration of 37.5 µg·mL⁻¹ was obtained for this treatment against both phytopathogens. Upon application via endotherapy on 20-year-old grapevines with clear esca and Botryosphaeria decay symptoms, no phytotoxicity effects were observed (according to SPAD and chlorophyll fluorescence measurements) and the sugar content of the grape juice was not affected either. Nonetheless, the treatment led to a noticeable decrease in foliar symptoms as well as a higher yield in the treated arms as compared to the control arms (3177 vs. 1932 g/arm), suggestive of high efficacy. Given the advantages in terms of controlled release and antimicrobial product savings, these biodegradable NCs loaded with natural extracts may deserve further research in large-scale field tests.

Keywords: *Equisetum arvense*; grapevine trunk diseases; natural bioactive products; NCs; *Rubia tinctorum*; *Silybum marianum*; *Urtica dioica*



Citation: Sánchez-Hernández, E.; Langa-Lomba, N.; González-García, V.; Casanova-Gascón, J.; Martín-Gil, J.; Santiago-Aliste, A.; Torres-Sánchez, S.; Martín-Ramos, P. Lignin–Chitosan Nanocarriers for the Delivery of Bioactive Natural Products against Wood-Decay Phytopathogens. *Agronomy* **2022**, *12*, 461. <https://doi.org/10.3390/agronomy12020461>

Academic Editors: Alain Deloire and Ivo Toševski

Received: 29 December 2021

Accepted: 10 February 2022

Published: 12 February 2022

Publisher's Note: MDPI stays neutral with regard to jurisdictional claims in published maps and institutional affiliations.



Copyright: © 2022 by the authors. Licensee MDPI, Basel, Switzerland. This article is an open access article distributed under the terms and conditions of the Creative Commons Attribution (CC BY) license (<https://creativecommons.org/licenses/by/4.0/>).

1. Introduction

Diseases associated with phytopathogenic microorganisms are responsible for important economic losses, affecting both arable crops (cereals, leguminous plants, vegetables, etc.) and woody crops (olive groves, vineyards, stone fruit and citrus orchards, etc.).

In the particular case of woody crops, the control of phytopathogens that cause diseases such as dieback and canker on economically and ecologically relevant host plants

poses a major challenge. For instance, grapevine trunk diseases (GTDs) are a representative example of the difficulties faced by wine-growers to control these pathogens using conventional pesticide applications [1]. Once a plant is infected, the pathogens segregate lignin-degrading enzymes (e.g., laccases and peroxidases) [2], which lead to trunk wood decay and withering of the plant. The pathogens' location inside the grapevine trunk hampers a facile application of antifungal treatments, such as conventional spraying [3]. To date, commercially available treatments are based on preventive measures, including permanent disinfection of pruning tools, protection of wounds on the vine, and repetitive preventive spraying of fungicides in high doses [1]. For progressed infections, the entire grapevine generally needs to be replaced [4] and, to prevent further spreading, removal and burning of the infected materials are essential.

Many of the synthetic agrochemicals traditionally employed to control these diseases (e.g., sodium arsenite) have been banned or public pressure has increased to reduce their use. The lack of effective curative treatments against GTDs has become a big threat to the European wine industry, causing an estimated financial loss of USD 1.5 B/year [5]. Therefore, the implementation of integrated pest management (IPM) methods has become a priority, either through the search for biocontrol agents (BCAs) or with the application of substances of natural origin [6], which need to be vehiculated into the plant's xylem.

The work presented herein focuses on the synthesis of biodegradable nanocarriers (NCs), based on methacrylated lignin (ML) and chitosan oligomers (COS), aimed at the targeted delivery of biologically active compounds (including hydrophobic ones). By incorporating lignin in their composition, the NCs can respond to external stimuli (viz. to the lignocellulolytic enzymes secreted by bacteria and fungi associated with wood diseases) at the sites of infection, triggering a controlled release of the therapeutic agents.

It is worth noting that lignin has been previously investigated as a renewable, abundant, and inexpensive feedstock to develop sophisticated nanostructures [7–9]. Lignin-derived compounds are useful as biodegradable building blocks for nanomaterials, and, in the past few years, some studies have presented lignin-based NCs [10]. Other bibliographic precedents include the work by Pathania et al. [11] on the preparation of a chitosan-g-poly(acrylamide) nanocomposites by a simple method in the presence of microwaves; the study by Beckers et al. [12] on the synthesis of xylan NCs employing toluene diisocyanate as a cross-linking agent (in which NCs were loaded with a synthetic fungicide); the investigations by Ciftci et al. [13] on the synthesis of chitosan microcapsules containing glycidyl methacrylate terpolymer, maleic anhydride, and *N*-*tert*-butylacrylamide, and some other articles on the formation of lignin–chitosan films [14,15]. However, to the best of the authors' knowledge, there are no reports on the insertion of chitosan oligomers between lignins (Aradmehr and Javanbakht [16] described lignin–chitosan biocomposites, but the existence of covalent interactions between the groups was not evidenced).

Concerning the bioactive products encapsulated in the NCs, other works have used conventional fungicides of chemical origin such as azoxystrobin, pyraclostrobin, tebuconazole, or boscalid [9,17], or BCAs, such as *Trichoderma reesei* E.G. Simmons [18]. As an alternative, this work proposes the use of plant extracts for which inhibitory concentrations below 1000 ppm against *Botryosphaeriaceae* species have been previously reported by our group, such as *Rubia tinctorum* L., *Silybum marianum* (L.) Gaertn., *Urtica dioica* L., or *Equisetum arvense* L. [19–21], and which have proven effective for pruning wound protection applications. These products of natural origin would be suitable for use in organic or conventional agriculture (in fact, the latter two are 'basic substances' under the EU plant protection products regulation, Article 23 of (EC) No 1107/2009).

As regards the phytopathogens chosen to test the efficacy of the NCs under study, *Neofusicoccum parvum* (Pennycook & Samuels) Crous, Slippers & A.J.L. Phillips is responsible for grapevine symptoms, such as leaf spots, fruit rots, shoot dieback, bud necrosis, vascular discoloration of the wood, and perennial cankers, and is considered one of the most aggressive species of the *Botryosphaeriaceae* family [22], which is why it was selected for the initial screening. Another member of the same group, *Diplodia seriata* De Not., was

also tested, given that it is considered a primary and virulent pathogen of grapevines [23], but it also causes frog-eye leaf spot, black rot, and canker of apples [24,25]. To determine the potential antibacterial activity, *Xylophilus ampelinus* Willems et al. (syn. *Xanthomonas ampelina* and *Erwinia vitivora*) [26] and *Pseudomonas syringae* pv. *syringae* van Hall were selected. The former is the causal agent of bacterial necrosis of grapevines (the so-called “maladie d’Oléron” in France and “mal nero” in Italy), which severely affects grape crops, resulting in harvest losses as high as 70% of typical yield [23], and is categorized as a quarantine A2 organism by the European and Mediterranean Plant Protection Organization (EPPO). The latter is a Gammaproteobacterium distributed worldwide, which is responsible for bacterial canker on over a hundred different hosts, including the grapevine (in which it induces necrotic lesions in the leaf blades, veins, petioles, shoots, rachis, and tendrils) [27].

In this work, we show the versatility of the ML–COS platform for the encapsulation of natural products with antimicrobial properties to treat GTDs and other plant diseases associated with lignin-decomposing microorganisms. The efficacy of the ML–COS NCs is first demonstrated in vitro against the four aforementioned phytopathogens, and the treatments are then assayed in *Vitis vinifera* plants by injection, resulting in a reduction in GTDs leaf symptoms. This strategy for drug delivery may help to optimize fungicide application and efficacy.

2. Materials and Methods

2.1. Plant Material and Reagents

The specimens of *Rubia tinctorum* and *S. marianum* under study were collected on the banks of the Carrión River as it passes through the town of Palencia (Spain). The roots of *R. tinctorum* were shade-dried and pulverized to a fine powder in a mechanical grinder. Samples from different specimens ($n = 25$) were thoroughly mixed to obtain composite samples. In the case of *S. marianum*, the capitula were collected during stage 67 (or 6N7) according to the extended BBCH scale, in which silybins precursors should not have yet been consumed, as discussed in previous work [21]. The capitula were shade-dried and pulverized to a fine powder in a mechanical grinder. Again, different specimens ($n = 25$) were thoroughly mixed to obtain a composite sample. For the preparation of *E. arvense* and *U. dioica* extracts, dried plants certified by the European Pharmacopoeia were purchased from El Antiguo Herbolario (Alicante, Spain).

Chitosan (CAS 9012-76-4; high molecular weight: 310,000–375,000 Da) was supplied by Hangzhou Simit Chem. & Tech. Co. (Hangzhou, China). Neutrase™ 0.8 L enzyme was supplied by Novozymes A/S (Bagsværd, Denmark). Potato dextrose agar (PDA) was supplied by Becton Dickinson (Bergen County, NJ, USA). DMF (Dimethylformamide, CAS 68-12-2), isopropyl alcohol (CAS 67-63-0), alkali lignin (CAS 8068-05-1), lithium chloride (CAS 7447-41-8), methacrylic anhydride (CAS 760-93-0), methanol (UHPLC, suitable for mass spectrometry, CAS 67-56-1), triethylamine (CAS 121-44-8), TSA (tryptic soy agar, CAS 91079-40-2), and TSB (tryptic soy broth, CAS 8013-01-2) were acquired from Sigma-Aldrich Química (Madrid, Spain).

2.2. Fungal and Bacterial Isolates

The two fungal isolates under study, *Neofusicoccum parvum* (code ITACYL_F111, isolate Y-091-03-01c) and *Diplodia seriata* (code ITACYL_F098, isolate Y-084-01-01a) were isolated from diseased grapevine plants of the cultivar ‘Tempranillo’ from D.O. Toro (Spain) and supplied as lyophilized vials (later reconstituted and refreshed as PDA subcultures) by the Instituto Tecnológico Agrario de Castilla y León (ITACYL, Valladolid, Spain).

Regarding the two bacterial isolates, *Xylophilus ampelinus* was acquired by the Spanish Type Culture Collection (CECT), with CCUG 21,976 strain designation, and *Pseudomonas syringae* pv. *syringae* was supplied by Aldearrubia Regional Diagnosis Center (Junta de Castilla y León, Spain).

2.3. Preparation of Plant Extracts

Extracts of *R. tinctorum* and *S. marianum* were obtained in a methanol:water mixture (1:1 *v/v*) according to the previously reported procedure [20,21]. In short, the dried samples were mixed with the hydromethanolic medium in a 1:20 (*w/v*) ratio and heated in a water bath at 50 °C for 30 min, followed by 5 min of sonication. The solutions were centrifuged at 9000 rpm for 15 min and the supernatants were filtered through Whatman No. 1 filter paper.

To obtain the *E. arvense* and *U. dioica* extracts, the procedures established in the European regulations (SANCO/12386/2013 and SANTE/11809/2016, respectively) were followed. In brief, in the case of horsetail extract, 200 g of the dried plant were macerated in 10 L of water for 30 min (soaking) and then boiled for 45 min. After cooling, the decoction was filtered and diluted by a factor of 10 with water to obtain a final concentration of 2 mg·mL⁻¹. For the nettle extract, dried nettle leaves (15 g·L⁻¹) were macerated for 3–4 days at 20 °C, followed by filtering and dilution of the filtrate to obtain a final concentration of 2 mg·mL⁻¹ [19].

The bioactive constituents present in each of the extracts, characterized by gas chromatography-mass spectroscopy (GC-MS), have been reported in previous works [19–21].

2.4. Procedure for the Synthesis of the Biodegradable Nanocarriers

Methacrylated lignin (ML) was first synthesized following the protocol reported by Fischer et al. [9] with slight modifications. The methacrylation of lignin was performed by the addition of methacrylic anhydride, which modifies the hydroxyl groups of lignin to make them available for the encapsulation of bioactive compounds. In short, 2.6 g LiCl was dissolved in 60 mL DMF, alternating periods of stirring and sonication until complete dissolution. Next, 2 g of Kraft lignin (total hydroxyl group content: 6.2 mmol·g⁻¹ determined by ³¹P NMR) was added, the mixture was stirred and sonicated until complete dissolution, under Ar atmosphere at 90 °C. The sample was cooled to 40–50 °C, and 1 mL of triethylamine (10 mmol) was added, then the mixture was stirred for 10 min. Subsequently, 3 mL of methacrylic anhydride (20 mmol) was added dropwise. The mixture was stirred at 60 °C for 6 h. The mixture was precipitated into a large excess of isopropyl alcohol and isolated by centrifugation, and the precipitation extraction procedure was repeated two more times. The product was dried at room temperature in a vacuum oven.

Chitosan oligomers (COS) were prepared according to the procedure described in the work by Santos-Moriano et al. [28], with the modifications indicated in [29]. Commercial chitosan ($M_W = 310\text{--}375$ kDa) was dissolved in aqueous 1% (*w/w*) acetic acid, and, after filtration, the filtrate was neutralized with aqueous 4% (*w/w*) NaOH. The precipitate was collected and washed thoroughly with hot distilled water, ethanol, and acetone. The purified chitosan was obtained by drying. The degree of deacetylation (DD) was determined to be 90% according to Sannan et al. [30]. A total of 20 g of purified chitosan were dissolved in 1000 mL of Milli-Q water by adding 20 g de citric acid under constant stirring at 60 °C. Once dissolved, the commercial proteolytic preparation Neutrase 0.8 L (a protease from *Bacillus amyloliquefaciens*) was added to obtain a product enriched in deacetylated chitoooligosaccharides and to degrade the polymer chains. The mixture was sonicated for 3 min in 1 min of sonication/1 min without sonication cycles to keep the temperature in the 30–60 °C range. The molar mass of the COS samples was determined by measuring the viscosity, in agreement with Yang et al. [31] in a solvent of 0.20 mol·L⁻¹ NaCl + 0.1 mol·L⁻¹ CH₃COOH at 25 °C using an Ubbelohde capillary viscometer. Molar mass was determined using the Mark–Houwink equation $[\eta] = 1.81 \times 10^{-3} M^{0.93}$ [32]. At the end of the process, a solution with a pH in the four to six interval with oligomers of molecular weight < 2 kDa was obtained, with a polydispersity index of 1.6, within the usual range reported in the literature [33].

The formation of the new nanocarriers loaded with bioactive plant extracts was conducted in two steps: (i) reaction of the amine of the chitosan oligomer with the methyl group of the methacrylated lignin, leading to the formation of an inclusion complex via the Aza-Michael reaction; (ii) interaction of the free hydroxyl groups of the COS with at

least one functional group of the constituents of the bioactive plant extracts, forming weak hydrogen bonds or ionic bonds. In short, 500 mg of ML (2.75 mmol methacrylic groups) were added to an aqueous solution of 250 mg (ca. 1.375 mmol NH₂ groups, considering a degree of deacetylation of 90%) of COS to cross-link it (i.e., 2:1 ML: COS stoichiometric ratio, chosen after testing different ratios), and then 50 mL of aqueous or methanol:water (1:1 *v/v*) plant extract were added. The mixture was emulsified by sonication at 20 kHz, in periods of 2 min each, and for a total time of 20 min, avoiding letting the temperature exceed 50 °C. The resulting emulsion was stirred for 12 h at 40 °C. Then, the final volume was adjusted to 50 mL, obtaining a concentration of the encapsulated bioactive compound of 2 mg·mL⁻¹.

Samples were purified by centrifugation at 10,000 rpm for 30 min. Next, the supernatant was frozen for 24 h and subsequently freeze-dried for study by attenuated total reflection Fourier-transform infrared spectroscopy (ATR-FTIR), thermal analysis, and transmission electron microscopy (TEM). Nanocarriers without active products were also freeze-dried for reference purposes.

An almost complete (over 95%) encapsulation efficiency was obtained for the four bioactive plant extracts tested. This encapsulation efficiency was determined using an indirect method, as in the work by Fischer et al. [9]. The sample was centrifuged at 10,000 rpm for 60 min and the supernatant containing the non-encapsulated plant extract was freeze-dried. The plant extract left was then dissolved in methanol:water (1:1, *v/v*), passed through a 0.2 µm filter and analyzed by high-pressure liquid chromatography (HPLC) with an Agilent 1200 series HPLC system (Agilent Technologies, Santa Clara, CA, USA) using methanol-5% acetic acid (pH 3) (70~30) as the mobile phase [34]. The injection volume was 10 µL and the column temperature was maintained at 20 °C. The analysis was conducted at a flow rate of 0.2 mL·min⁻¹ with the G1315D detector operated at 250 nm. The encapsulation efficiency (EE) was determined according to the following equation:

$$EE(\%) = \frac{m(\text{bioactive product initial}) - m(\text{bioactive product supernatant})}{m(\text{bioactive product initial})} \times 100$$

2.5. Characterization of the Nanocarriers

To confirm the cross-linkage between ML and COS, ATR-FTIR was used. Infrared vibrational spectra were recorded using a Thermo Scientific (Waltham, MA, USA) Nicolet iS50 FTIR spectrometer equipped with an integrated diamond ATR system. The spectra were registered with a spectral resolution of 1 cm⁻¹ in the range 400–4000 cm⁻¹, taking the interferograms that resulted from the co-addition of 64 scans. The spectra were then corrected using the advanced ATR correction algorithm available in the OMNICTM software suite.

Thermal gravimetry (TGA) and differential scanning calorimetry (DSC) analyses were carried out using a simultaneous TG-DSC2 (Mettler Toledo; Columbus, OH, USA), in 'atmosphere of synthetic air' (N₂:O₂ in 4:1 ratio), with a heating ramp of 20 °C·min⁻¹. It should be clarified that the choice of the atmosphere would only influence the activation energy values [35].

Additional characterization of the NCs was carried out by dynamic light scattering (DLS), zeta potential (ZP), and transmission electron microscopy (TEM) at the Laboratory of Instrumental Techniques (LTI) of Universidad de Valladolid. The nanoparticle size distribution was evaluated by DLS using a Zetasizer Advance Pro Red Label apparatus (Malvern Panalytical Ltd., Malvern, UK), with a laser wavelength of 633 nm (He-Ne, 10 mW) and a 175° scattering angle. The zeta potential of nanoparticles was measured on a zeta potential analyzer (Brookhaven, GA, USA). For zeta potential measurements, samples were diluted with 0.1 mM KCl and measured in the automatic mode. DLS and ZP measurements were conducted in triplicate. TEM characterization was conducted using a JEOL (Akishima, Tokyo, Japan) JEM 1011 microscope. Operative conditions: 100 kV; 25,000–120,000× magnification. Micrographs have been obtained with a GATAN ES100W CCD camera (4000 × 2672 pixels).

2.6. In Vitro Antimicrobial Activity Assessment

The antifungal activity of the different treatments was determined by the agar dilution method according to the EUCAST antifungal susceptibility testing standard procedures [36], by incorporating aliquots of NCs, either empty or loaded with the different plant extracts, into PDA medium to obtain concentrations in the 6.25–150 $\mu\text{g}\cdot\text{mL}^{-1}$ range. Fungal mycelial plugs ($\phi = 5$ mm) from the margins of 1-week-old *N. parvum* and *D. seriata* colonies were transferred onto plates that incorporated the above concentrations for each treatment (3 plates per treatment/concentration, with 2 replicates each). Plates were then incubated at 25 °C in the dark for 1 week. PDA medium without any modification was used as a control. Mycelial growth inhibition was estimated according to the formula $(d_c - d_t)/d_c \times 100$, where d_c and d_t represent the mean diameters of the control and treated fungal colony, respectively. The effective concentrations at which mycelial growth was inhibited by 50 and 90% (EC₅₀ and EC₉₀, respectively) were estimated using PROBIT analysis in IBM SPSS Statistics v.25 software (IBM; Armonk, NY, USA).

The antibacterial activity was assessed according to CLSI standard M07–11 [37], using the agar dilution method to determine the minimum inhibitory concentration (MIC). In short, an isolated colony of *X. ampelinus* in a TSB liquid medium was incubated at 26 °C for 24 h. Serial dilutions were then conducted, starting from a 10^8 CFU·mL⁻¹ concentration, to obtain a final inoculum of $\sim 10^4$ CFU·mL⁻¹. Bacterial suspensions were then delivered to the surface of TSA plates, to which the treatments had previously been added at concentrations ranging from 6.25 to 150 $\mu\text{g}\cdot\text{mL}^{-1}$. Plates were incubated at 26 °C for 24 h. Readings were taken after 24 h. In the case of *P. syringae* pv. *syringae*, the same procedure was followed, albeit at 25 °C for 48 h. MICs were visually determined in the agar dilutions as the lowest concentrations of the bioactive products at which no bacterial growth was visible. All experiments were run in triplicate, with 3 plates per treatment/concentration.

2.7. In Planta Application of ML–COS NCs-Based Treatments

Bioassays with the ML–COS NCs treatment that showed the best performance at lab scale (viz. NCs loaded with *R. tinctorum* extract) were performed by injection (via endotherapy) in vines with clear symptoms of GTDs. A total of 20 grapevines of cultivar ‘Cabernet sauvignon’ grafted on SO4 rootstock, planted in 2000 on the ‘Clau’ estate of the Viñas del Vero winery (Somontano Designation of Origin Barbastro, Huesca, Spain) were used for the tests. Only plants in which both arms were clearly affected by GTDs (verified in previous years by the winery) were selected for this study (Figure 1).

In addition to the information provided by the winery, the phytosanitary status of the plot subjected to treatment was analyzed through the isolation and characterization of fungal pathogens associated with plants that showed the aforementioned symptoms compatible with the existence of GTDs, especially at the level of rot and decay of lignified tissues in arms. Briefly, these materials were fragmented, surface-sterilized (employing 70% ethanol, 5% commercial sodium hypochlorite, and sterile double distilled water), and incubated in Petri dishes containing PDA as nutritive medium and streptomycin sulfate to prevent bacterial contamination at 26 °C in the dark for 3–5 days. After this, the different emerging colonies were transferred to PDA plates as pure colonies and characterized both at the morphological level (through the microscope study of their morphological characters in culture) and by using molecular methods (through the obtaining and subsequent comparison of their ribosomal ITS sequences).



Figure 1. Upper row: examples of grapevine trunk diseases wood symptoms in the plants used for the in vivo study; lower row: inoculation point with a plug installed and injection of the treatment.

The treatment was injected into one of the arms (randomly chosen) of each symptomatic and diseased vine, using the other arm as a control. The arm site selected for the injection was first sprayed with 5% sodium hypochlorite to sterilize the wood surface. Subsequently, a 20 mm deep hole was drilled, in which a plug with a non-return valve was installed (Figure 1). The drill bit was sterilized with 70% ethanol before drilling the next plant. The injection system (ENDOkit Manual™, developed by ENDOTerapia Vegetal, Gerona, Spain) was then loaded with 5 mL of the corresponding nanocarrier ML-COS-*R. tinctorum* solution. It was not necessary to seal the wound with wax to avoid contamination due to the type of plug (ENDOplug™) used in the selected endotherapy system. The second injection application of the treatment was carried out a month later using the same injection site, so the same plug could be used (given that it had not been clogged with scar tissue yet). The monitoring of the plants lasted for 5 months.

Measurements of fast chlorophyll fluorescence induction kinetics were carried out using a continuous excitation chlorophyll fluorimeter (model Handy PEA+, Hansatech Instruments, Pentney, Norfolk, UK), on a bimonthly basis throughout the vegetative period (from late May till the beginning of September). Five measurements were taken on each arm of the twenty plants under study, to investigate subtle differences in the fluorescence signature of samples, which could be indicative of stress factors affecting the photosynthetic efficiency of the plant. The ratio of the variable fluorescence (F_v) over the maximum fluorescence value (F_m) was chosen as an indicator of the maximum quantum efficiency of Photosystem II, being a sensitive indication of plant photosynthetic performance. Presented as a ratio between 0 and 1, healthy samples typically achieve a maximum F_v/F_m value of approx. 0.85, while lower values suggest that the plant has been exposed to some type of biotic or abiotic stress factor. Leaf chlorophyll status was also monitored bimonthly throughout the entire vegetative period (May–September). A SPAD-502 m (Minolta, Osaka, Japan) was used. Five values were collected for each arm.

Upon grape harvest, the productivity of the treated and control arms was compared by recording both the number of bunches per arm and their fresh weight, provided that the pruning criterion was homogeneous in all the grapevines under study and that no cluster thinning was conducted. The approximate sugar content of the obtained grape

juice—a parameter used by the winery to determine the optimum time for harvesting—was analyzed using a PCE-032 refractometer (PCE Ibérica SL, Albacete, Spain) in order to investigate possible differences in the phenological state, relating berry maturity to the presence of disease in the arm that supported them.

2.8. Statistical Analysis

The results of in vitro mycelial growth inhibition were statistically analyzed by analysis of variance (ANOVA), followed by a post hoc comparison of means by Tukey's test (because the requirements of homogeneity and homoscedasticity were met, according to the Shapiro–Wilk and Levene tests). For the results of the field tests, non-parametric analyses were carried out with the Kruskal–Wallis test, accompanied by the comparison of pairs with the Dunn and Conover–Iman methods, applying the Bonferroni correction.

3. Results

3.1. Characterization by ATR-FTIR

Methacrylated lignin presents a weak band at 1397 cm^{-1} , which increased and split into two bands after the formation of the ML–COS NCs, with peaks at 1417 and 1396 cm^{-1} (Figure S1). With regard to the chitosan oligomers, they present two bands at 1062 and 1031 cm^{-1} that drastically decreased with the formation of the ML–COS NCs (with a concurrent shift towards 1107 and 1037 cm^{-1}). This corresponds to a decrease in the C=C bands of the vinyl groups due to their consumption during the Aza–Michael cross-linking polymerization, which was accompanied by the appearance of -NH bands at 1570 cm^{-1} [17]. Further, the increase in the vibrations of the ester bond at 1652 cm^{-1} (-C=O) and of the hydroxyl group (-OH) at 3377 cm^{-1} point to successful incorporation of COS into methacrylic groups of lignin.

On the other hand, in the spectra corresponding to ML–COS NCs loaded with *R. tinctorum* extracts (Figure S2) it was observed how the weak -NH band of the *R. tinctorum* extract at 1591 cm^{-1} overlapped with the 1570 cm^{-1} NH band of the ML–COS NCs to give rise to a very intense band at 1571 cm^{-1} .

3.2. Characterization by Thermal Analysis

The TGA curves for the ML–COS NCs (without encapsulated extracts), with a basic ML–COS–ML structure, showed high stability: below 200 °C a weight loss of 9% occurred and, from this temperature up to 750 °C , an additional 7% weight loss was registered. The maximum decomposition took place at 350 °C and was sensitized by the presence of an exotherm (Figure S3). The ML–COS–ML NC was, therefore, more stable than the lignin–diamine–lignin analogs reported to date [9,17]: the curves of ML–diamine–ML type NCs, presented in Figure S4, show that they experience weight losses of up to 37% at 350 °C due to lignin degradation (sensitized by an exotherm at 260 °C).

The curves for ML–COS NCs loaded with *R. tinctorum*, showed, upon heating up to 500 °C , three successive stages of decomposition with associated weight losses of 12, 30, and 10%, respectively. At higher temperatures, an exotherm was observed at 510 °C and, at the end of the process (at 750 °C), a 28% weight loss, in addition to the previous ones, was recorded (Figure S5). This thermal behavior was thus very different from that of the empty NCs and should be referred, fundamentally, to the presence of the *R. tinctorum* components inside the ML–COS–ML encapsulation.

3.3. Characterization by Transmission Electron Microscopy, Dynamic Light Scattering, and Zeta Potential

Figure 2 shows TEM micrographs of the nanocarriers. The addition of the plant extracts to the miniemulsion did not result in a significant change of the NCs size, compared to empty NCs, a result consistent with those reported by Fischer et al. [9].

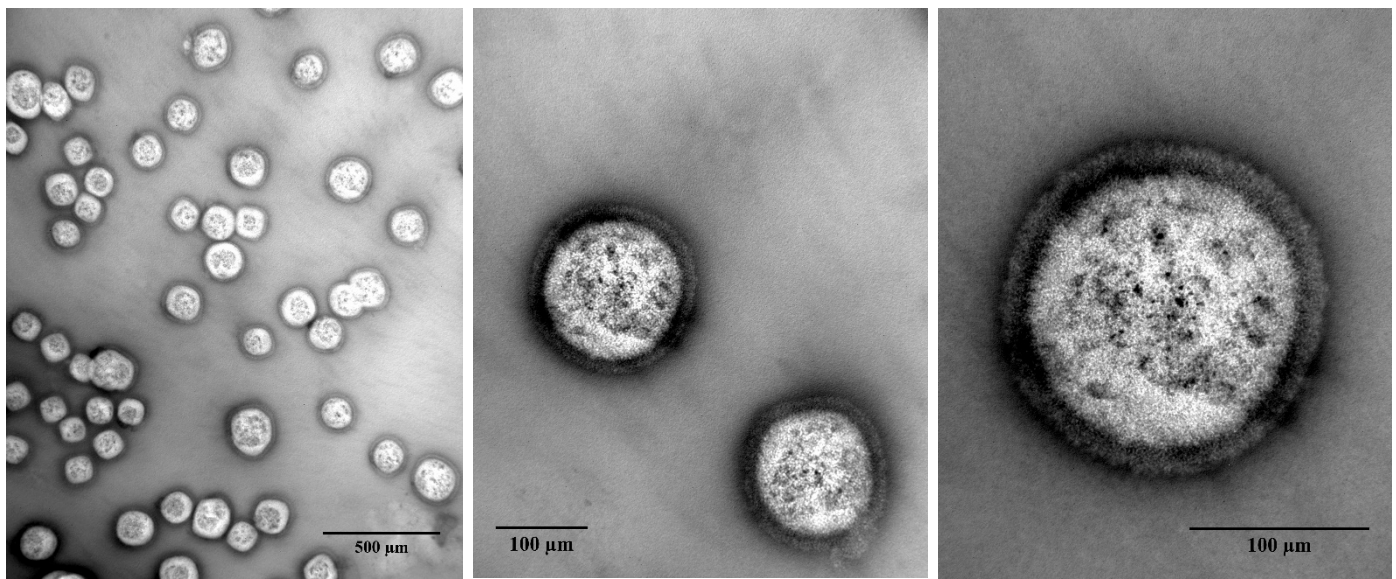


Figure 2. Transmission electron microscopy (TEM) images showing the ML-COS NCs loaded with *R. tinctorum* extract at different magnifications.

The average particle size ($D_p = 185$ nm; PDI = 0.35), determined by DLS, was on the lower end of the range reported by Machado et al. [17] (165–300 nm) and slightly smaller than those reported by Fischer et al. [9] (213–510 nm) for lignin NCs. The number distribution of ML-COS-*R. tinctorum* NCs showed that 99% of particles had sizes lesser than 200 nm, which included: 162.9 nm (19.29%), 185.7 nm (57.7%), and 209.1 nm (22.3%). The obtained PDI value, below 0.5, indicates that particles were monodispersed in nature, and suggests uniformity and stability of particles in suspension, according to Choudhary et al. [38].

Regarding the zeta potential, a +42 mV value was obtained, in the usual range for chitosan nanomaterials (+22 to +88 mV) [39] and above the 20 mV threshold required for colloidal stability [40].

3.4. In Vitro Antimicrobial Activity

3.4.1. Antifungal Activity

The visual results of the mycelial growth inhibition tests of *N. parvum* and *D. seriata* are shown in Figure S6.

Inhibition of *N. parvum* mycelial growth (Figure 3) was achieved at concentrations as low as 75 and 100 $\mu\text{g}\cdot\text{mL}^{-1}$ for the NCs loaded with the extracts of *R. tinctorum* and *S. marianum*, respectively, while the minimum inhibitory concentrations (MICs) for the encapsulated *E. arvense* and *U. dioica* extracts were higher (150 $\mu\text{g}\cdot\text{mL}^{-1}$ in both cases).

Due to the good results obtained with the NCs loaded with the *R. tinctorum* extract, these were further tested against another fungal pathogen of the *Botryosphaeriaceae* family, viz. *D. seriata* (Figure 4). In its case, the NCs loaded with *R. tinctorum* inhibited mycelial growth at a concentration of 100 $\mu\text{g}\cdot\text{mL}^{-1}$.

Regarding effective concentrations, Table 1 summarizes the EC_{50} and EC_{90} values obtained against *N. parvum* for NCs, either empty or loaded with the different bioactive compounds, together with the results obtained with unencapsulated extracts (for comparison purposes). A clear improvement in terms of activity was observed in all cases, with EC_{50} and EC_{90} as low as 41.2 and 65.8 $\mu\text{g}\cdot\text{mL}^{-1}$, respectively, for the NCs loaded with *R. tinctorum* extract.

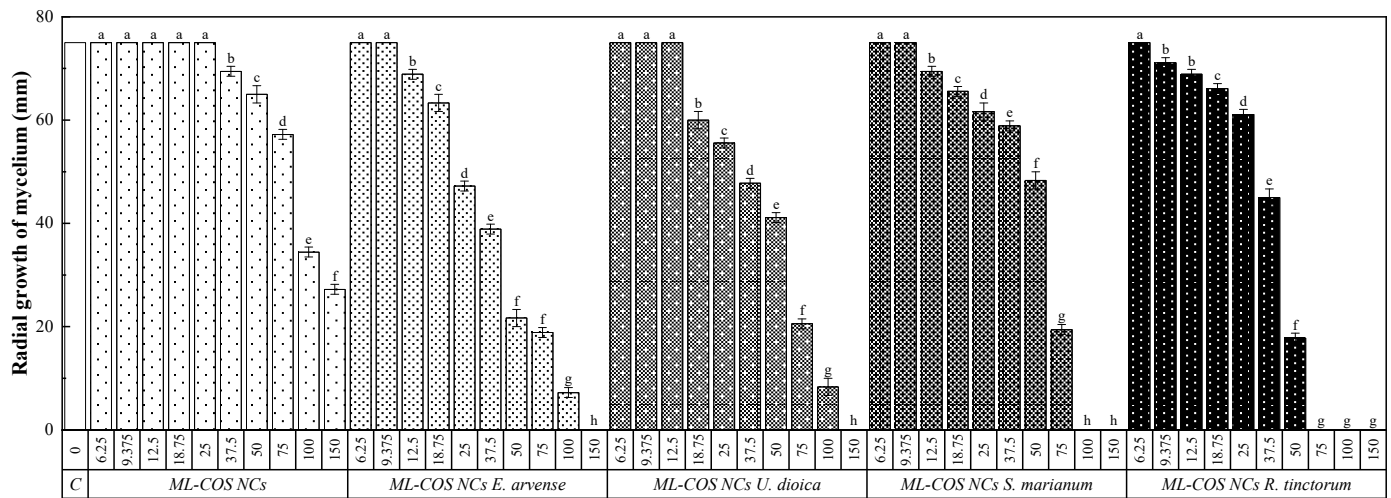


Figure 3. Diameter of *N. parvum* radial mycelial growth upon treatment with ML–COS NCs, either empty or loaded with four plant extracts at different concentrations (6.25; 9.375; 12.5; 18.75; 25; 37.5; 50; 75; 100; 150 $\mu\text{g}\cdot\text{mL}^{-1}$). Same letters above concentrations mean not significantly different at $p < 0.05$. Error bars represent standard deviations.

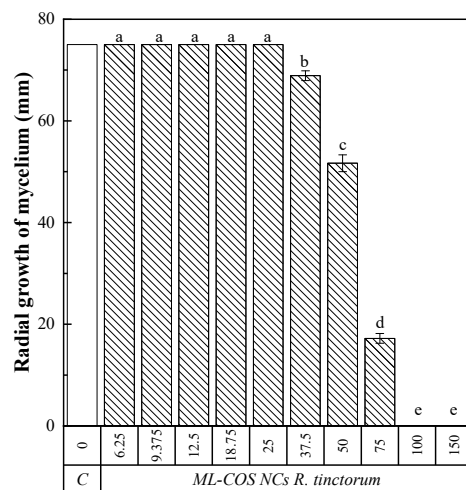


Figure 4. Diameter of *D. seriata* radial mycelial growth upon treatment with ML–COS NCs loaded with *R. tinctorum* extract at different concentrations (6.25; 9.375; 12.5; 18.75; 25; 37.5; 50; 75; 100; 150 $\mu\text{g}\cdot\text{mL}^{-1}$). Same letters above concentrations mean not significantly different at $p < 0.05$. Error bars represent standard deviations.

Table 1. EC₅₀ and EC₉₀ concentrations against *N. parvum* of the ML–COS NCs, with or without encapsulated bioactive products, expressed in $\mu\text{g}\cdot\text{L}^{-1}$. Effective concentrations of the non-encapsulated products are provided for comparison purposes.

Effective Concentration	ML–COS	NC-Based Treatments				COS	Non-Encapsulated Products [19–21]			
		ML–COS– <i>E. arvense</i>	ML–COS– <i>U. dioica</i>	ML–COS– <i>S. marianum</i>	ML–COS– <i>R. tinctorum</i>		<i>E. arvense</i>	<i>U. dioica</i>	<i>S. marianum</i>	<i>R. tinctorum</i>
EC ₅₀	82.7	66.5	50.2	60.9	41.2	680.2	*	*	557	92.3
EC ₉₀	243.2	105.2	113.0	90.6	65.8	1326.6	*	*	2938	184.0

* No inhibition of mycelial growth was observed at 1500 $\mu\text{g}\cdot\text{mL}^{-1}$, the highest concentration tested.

Regarding the EC₅₀ and EC₉₀ values obtained against *D. seriata* (Table 2), the *R. tinctorum* extract encapsulated in the NCs presented a lower EC₅₀ than that of the non-encapsulated extract, although the EC₉₀ value was similar in both cases.

Table 2. EC₅₀ and EC₉₀ concentrations against *D. seriata* of the ML–COS NCs loaded with *R. tinctorum* extract and of the non-encapsulated extract, expressed in µg·L⁻¹.

Effective Concentration	Encapsulated Product ML–COS– <i>R. tinctorum</i>	Non-Encapsulated Product <i>R. tinctorum</i>
EC ₅₀	59.3	78.0
EC ₉₀	91.0	87.8

3.4.2. Antibacterial Activity

The efficacy of the most effective treatment in the antifungal in vitro tests, ML–COS–*R. tinctorum*, was assayed against two phytopathogenic bacteria, *P. syringae* pv. *syringae* and *X. ampelinus*, to investigate if these biodegradable NCs could have a wider spectrum of action against other microorganisms, not only restricted to eukaryotic plant pathogens. The inhibition attained against the two bacteria with the NCs loaded with *R. tinctorum* extract were similar, with a MIC value of 37.5 µg·mL⁻¹ (Table 3).

Table 3. Antibacterial activity of ML–COS–*R. tinctorum* treatment against the two phytopathogenic bacteria under study at different concentrations (expressed in µg·mL⁻¹).

Pathogen	Concentration									
	6.25	9.75	12.5	18.75	25	37.5	50	75	100	150
<i>P. syringae</i> pv. <i>syringae</i>	+	+	+	+	+	–	–	–	–	–
<i>X. ampelinus</i>	+	+	+	+	+	–	–	–	–	–

“+” and “–” indicate the presence and absence of bacterial growth, respectively.

3.5. In Planta Application of ML–COS NCs Loaded with *R. tinctorum* Extract Treatment

After the morphological and molecular characterization of the isolates obtained from samples from symptomatic plants of the treated plot, the majority presence of species associated with GTDs such as the lignicolous basidiomycete species *Fomitiporia mediterranea* M. Fisch. or, with a greater frequency of appearance, certain *Botryosphaeriaceae* species such as *Diplodia seriata* or *Neofusicoccum parvum*, was verified.

When GTDs-associated foliar symptoms were monitored, most of the treated arms showed less interveinal chlorosis and necrosis than their respective control arms (Figure 5). Nonetheless, given that foliar symptoms associated with GTDs do not necessarily appear on the same diseased plant every year, other approaches were used to estimate the preliminary efficacy of the treatment.

**Figure 5.** Examples of decrease in foliar GTD symptoms in treated vs. non-treated grapevine arms.

Concerning SPAD and fluorometry measurements, always conducted on healthy leaves (not on leaves with chlorosis or necrosis symptoms), no statistically significant differences were detected between the treated and control arms, ruling out relevant phytotoxic effects of the treatment performed.

With regard to the yield measurements, significant differences (p -value = 0.047) were found in the number of clusters, with 39 ± 11.4 and 24.6 ± 9.1 clusters/arm in the treated vs. non-treated arms, respectively. This difference in the number of clusters did not lead to significant differences in the yield per arm (p -value = 0.117), although it was noticeably higher in the treated arms than in the control ones (3177 ± 1259 vs. 1932 ± 556 g/arm, respectively).

In relation to the probable sugar content of the grape juice, it was shown to be similar in both treated and control arms (22.0 ± 1.8 vs. 21.2 ± 1.6 °Bx), discarding differences in berry maturity.

4. Discussion

4.1. Comparison with Other NCs-Based Treatments

A summary of other research works reported in the literature in which NCs have been used to control diseases associated with wood-degrading fungi is presented in Table 4.

Table 4. Summary of NCs-based treatments reported in the literature against wood-degrading fungi.

Composition	Pathogen	Assays	Ref.
Kraft cationic lignin NCs loaded with <i>Trichoderma reesei</i> spores	Fungi associated with GTDs (esca)	Dual in vitro culture against <i>Phaeoconiella chlamydospora</i> and <i>Phaeoacremonium minimum</i> + in vitro NC degradation assays with culture filtrate of the two esca pathogens	[18]
Methacrylated Kraft lignin NCs loaded with pyraclostrobin	Fungi associated with GTDs (esca)	Field study with trunk injections in <i>V. vinifera</i> plants	[9]
Methacrylated Kraft lignin NCs loaded with different synthetic fungicides (pyraclostrobin, azoxystrobin, tebuconazole, boscalid)	Ligninase-producing microorganisms	In vitro antifungal activity against <i>P. chlamydospora</i> , <i>Neonectria ditissima</i> , <i>Phytophthora infestans</i> , <i>Magnaporthe oryzae</i> , <i>Botrytis cinerea</i> , <i>N. parvum</i> + in planta study through trunk injections in <i>V. vinifera</i> plants	[17]
Pyraclostrobin-loaded xylan NCs	Xylanase-producing fungi in viticulture and horticulture	In vitro assays against <i>Pyricularia oryzae</i> , <i>B. cinerea</i> , <i>P. chlamydospora</i> , <i>P. minimum</i> , and <i>N. ditissima</i>	[12]
Cellulose modified with undec-10-enoic acid NCs loaded with pyraclostrobin and captan	Cellulase segregating fungi in viticulture and apple trees	In vitro assays against <i>P. chlamydospora</i> , <i>N. ditissima</i> , <i>P. infestans</i> , <i>M. oryzae</i> , <i>B. cinerea</i> , and <i>N. parvum</i>	[41]

From a chemical perspective, the main difference between the NCs presented in this work and those based on lignin reported by other authors (e.g., the NCs protected by patent WO 2017/134308 A1 [42], tested in [9,17]) is that the latter are based on ML–diamine–ML networks (while the NCs reported herein are based on ML–COS–ML networks). In ML–diamine–ML networks, the space generated for the accommodation of the active compounds is of discrete dimensions and may not allow to stably accommodate large molecules, apart from the fact that the addition of the bioactive compounds would take place in a hydrophobic medium, which conditions bioavailability. Thus, the use of COS instead of diamines should facilitate the entry and encapsulation of large bioactive compounds such as flavonoids, di- and triterpenes, given that COS presents a large number of functional groups, such as hydroxyl and amino, and is considered a polycation with a high density of positive charges ideal for interacting with bioactive compounds. Hence, the formation of inclusion compounds between the ML–COS–ML shell and the encapsulated natural products shall not be excluded. Further, the NCs should also function more effectively as an antimicrobial upon the incorporation of chitosan, due to its non-specific mechanism of pathogen suppression (COS permeabilizes fungal plasma membranes and alters their gene expression), although it can be anticipated that the methacrylated COS used in the NCs will not have the same activity as free COS.

With regard to the efficacy of the treatments, the susceptibility profile is usually considered isolate-dependent, so comparisons of the effective concentrations below should be taken with caution. For instance, Machado et al. [17] reported MIC values against *N. parvum* of 5 and $>50 \mu\text{g}\cdot\text{mL}^{-1}$ for lignin NCs cross-linked with 2,2'-(ethylenedioxy)bis(ethylamine) (EDBEA) loaded with 30 wt% azoxystrobin or pyraclostrobin, and with boscalid or tebuconazole, respectively, similar to those attained for bulk fungicide formulations. For *P. chlamydospora*, MICs of $5 \mu\text{g}\cdot\text{mL}^{-1}$ were found in all cases. Comparable MICs $< 10 \mu\text{g}\cdot\text{mL}^{-1}$

against *P. chlamydospora* and *Phaeoacremonium aleophilum* were also reported by the same group for pyraclostrobin xylan-based nanocarriers [12]. When cellulose-based NCs loaded with pyraclostrobin (20–30 wt%) and captan (20–30 wt%) were used instead, MICs of 5 and $>50 \mu\text{g}\cdot\text{mL}^{-1}$ were obtained, respectively [41]. Hence, taking into consideration that the EC_{90} value reported herein for the ML–COS NCs loaded with *R. tinctorum* extract against *N. parvum* was $65.8 \mu\text{g}\cdot\text{mL}^{-1}$, the efficacy would be worse than that of azoxystrobin or pyraclostrobin and higher than that of boscalid, tebuconazole or captan.

Concerning the antibacterial activity, no tests were conducted for any of the NCs presented in Table 4, but it is worth noting that the MIC value attained against *P. syringae* for the ML–COS NCs loaded with *R. tinctorum* extract ($37.5 \mu\text{g}\cdot\text{mL}^{-1}$) was substantially lower than, for instance, the one reported by Tang et al. [43] ($\text{MIC} = 106.25 \mu\text{g}\cdot\text{mL}^{-1}$) for self-assembled nanoparticles based on polyhexa-methylene biguanide (PHMB) and fenhexamid (FHA) fungicide against *Pseudomonas syringae* pv. *lachrymans*.

In relation to in vivo studies, Fischer et al. [9] studied the effect of lignin NCs loaded with pyraclostrobin ($700 \mu\text{g}\cdot\text{mL}^{-1}$) on 43 grapevine plants. They observed a significant improvement in their conditions after 3 months and up to 4 years, occurring less or even no leaf symptoms, while treatment with non-encapsulated F500 pyraclostrobin-based commercial product (BASF) at a higher dose ($6000 \mu\text{g}\cdot\text{mL}^{-1}$) resulted in an initial improvement of the symptoms, but the symptom level increased again in the following years. In another study by the same group, Machado et al. [17] tested the long-term antifungal effect over a 4-year period on four *V. vinifera* cv. “Portugieser” plants treated with 5 mL of a 1 wt% dispersion of lignin NCs loaded with boscalid. Although the number of specimens was small, they observed almost no signs of esca in the boscalid NC treated plants, which was attributed to a slower degradation in planta or a possible depot effect that lasts for several years. In the study presented herein, the referred initial improvement was also observed, with a reduction of leaf symptoms, but the long-term efficacy has not been determined yet (the plants are still under observation for the next years).

The principle of operation would be similar in the three cases: the NCs are introduced by trunk injection, and transported along the plant, via xylem (upward movement) and phloem (downward movement), from the injection site to reach the infected tissues [9]. The lignin-based encapsulation inhibits the undesired premature release of the bioactive product (a synthetic fungicide in most cases, or *T. reesei* conidia in the work by Peil et al. [18]) and enables the application as an aqueous dispersion via trunk injection. When lignin-degrading fungi infect the plant, enzymatic degradation of the lignin-based shell occurs and the release of the fungicide is selectively triggered by the pathogenic fungi itself.

4.2. Limitations of the Study

Several limitations of the study should be brought to the reader’s attention. Firstly, the in vivo study was conducted in a single location over a single annual growth cycle. Hence, multi-year and multi-location tests would be needed to confirm the good performance of the treatment reported in this work. Optimization of the dispersion properties and dosage should also be addressed in future bioassays.

Secondly, the chosen application procedure by endotherapy would not be a suitable solution for all the GTDs-related scenarios that may be found in most wineries: (i) it requires that symptomatic plants have been previously identified, which implies that the GTDs may already be in an advanced state; (ii) the application is time-consuming (approximately 5 min/plant, considering the time required to drill the hole, insert the plug and inject the solution), so it may not be cost-effective unless the treated plants are used to produce quality wines (as it was the case in the chosen state); (iii) the plugs—which remain in the plant—cannot be reused for subsequent injections, as they are eventually clogged by the scar tissue; (iv) the depth of the drilling hole (20 mm) does not allow application of the treatments in young grapevine plants. It should be clarified that this latter point would not be an issue if the treatment was to be applied to trees.

5. Conclusions

In in vitro mycelial growth inhibition tests, the nanocarriers loaded with *R. tinctorum* extract were highly effective against *N. parvum*, with EC₅₀ and EC₉₀ concentrations of 41.2 and 65.8 µg·mL⁻¹, respectively (lower than those obtained for NCs loaded with *S. marianum*, 60.9 and 90.6 µg·mL⁻¹; *E. arvense*, 66.5 and 105.2 µg·mL⁻¹; and *U. dioica*, 50.2 and 113.0 µg·mL⁻¹, respectively). Hence, it was further assayed against other wood-degrading pathogens: EC₅₀ and EC₉₀ concentrations of 59.3 and 91.0 µg·mL⁻¹, respectively, were found against *D. seriata*, and a MIC of 37.5 µg·mL⁻¹ was obtained against *X. ampelinus* and *P. syringae* pv. *syringae*, respectively. Subsequently, it was evaluated in field conditions, in which it was applied by endotherapy to 20-year-old grapevines with clear GTD symptoms. SPAD and chlorophyll fluorescence measurements did not suggest any phytotoxicity effects associated with the treatment, and the sugar content of the grape juice was not affected either. Nonetheless, the NCs-based treatment led to a noticeable decrease in foliar symptoms, statistically significant differences in the number of bunches per arm, and a noticeably higher yield in the treated arms as compared to the control arms (3177 vs. 1932 g/arm), pointing to a high efficacy. Given the advantages of these ML-COS NCs over other systems for the delivery of bioactive compounds in phytosanitary applications due to the exclusive use of natural polymers (instead of synthetic cross-linking amines and organic solvents), together with a reduction in the amount of bioactive compound to be used and the feasibility of a controlled release, they hold promise for the effective and safe application of integrated control treatments against wood-degrading pathogens.

6. Patents

The work reported in this manuscript is related to the Spanish patent with application number P202131019 ('Compuesto reticulado de lignina metacrilada y oligómeros de quitosano capaz de actuar como nanotransportador de compuestos bioactivos, método de obtención y usos'; 'Cross-linked compound of methacrylated lignin and chitosan oligomers capable of acting as a nanocarrier of bioactive compounds, method of obtaining and uses' (tr.)), filed on 29 October 2021.

Supplementary Materials: The following are available online at <https://www.mdpi.com/article/10.3390/agronomy12020461/s1>, Figure S1: Comparison of the ATR-FTIR spectra of the ML-COS nanocarriers; lignin NCs with synthetic amine cross-linking prepared according to the procedure reported by Fischer et al.; enzymatically obtained chitosan oligomers. Figure S2: Comparison of the ATR-FTIR spectra of the ML-COS NCs loaded with *R. tinctorum* extract, ML-COS NCs with no encapsulated product, and the lyophilized *R. tinctorum* extract. Figure S3: Thermal analysis of the ML-COS nanocarriers. Figure S4. Thermal analysis of ML-diamine-ML nanocarriers prepared according to the procedure reported by Fischer et al. Figure S5. Thermal analysis of the ML-COS nanocarriers loaded with *R. tinctorum* extracts. Figure S6. Effect ML-COS NCs-based treatments at different concentrations on the mycelial growth of *N. parvum* and *D. seriata*, respectively.

Author Contributions: Conceptualization, J.M.-G., P.M.-R. and V.G.-G.; methodology, J.M.-G., J.C.-G., S.T.-S. and V.G.-G.; validation, J.C.-G., V.G.-G. and P.M.-R.; formal analysis, J.C.-G., V.G.-G. and P.M.-R.; investigation, E.S.-H., N.L.-L., V.G.-G., J.C.-G., J.M.-G., A.S.-A. and P.M.-R.; resources, J.M.-G., S.T.-S. and P.M.-R.; data curation, J.C.-G.; writing—original draft preparation, E.S.-H., N.L.-L., V.G.-G., J.C.-G., J.M.-G., S.T.-S. and P.M.-R.; writing—review and editing, E.S.-H., V.G.-G., J.M.-G., A.S.-A. and P.M.-R.; visualization, N.L.-L., E.S.-H. and A.S.-A.; supervision, V.G.-G. and P.M.-R.; project administration, J.M.-G. and P.M.-R.; funding acquisition, J.M.-G. and P.M.-R. All authors have read and agreed to the published version of the manuscript.

Funding: This research was funded by Junta de Castilla y León under project VA258P18, with FEDER co-funding by Cátedra Agrobank under the "IV Convocatoria de Ayudas de la Cátedra AgroBank para la transferencia del conocimiento al sector agroalimentario" program and by Fundación Ibercaja-Universidad de Zaragoza under the "Convocatoria Fundación Ibercaja-Universidad de Zaragoza de proyectos de investigación, desarrollo e innovación para jóvenes investigadores" program.

Institutional Review Board Statement: Not applicable.

Informed Consent Statement: Not applicable.

Data Availability Statement: The data presented in this study are available on request from the corresponding author. The data are not publicly available due to their relevance to an ongoing Ph.D. thesis.

Acknowledgments: To Fundación General de la Universidad de Valladolid, for funding the patent through the ‘Prometeo’ program. To José M. Ayuso-Rodríguez and Adrián Jarné-Casasús, from Viñas del Vero S.A. winery. The authors also gratefully acknowledge the support of Pilar Blasco and Pablo Candela at the Servicios Técnicos de Investigación, Universidad de Alicante, for conducting the GC-MS analyses, and wish to thank José Luis Palomo Gómez, from the Aldearrubia Regional Diagnostic Center (Junta de Castilla y León) for providing the *P. syringae* pv. *syringae* isolate used in the study.

Conflicts of Interest: The authors declare no conflict of interest.

References

1. Mondello, V.; Songy, A.; Battiston, E.; Pinto, C.; Coppin, C.; Trotel-Aziz, P.; Clément, C.; Mugnai, L.; Fontaine, F. Grapevine trunk diseases: A review of fifteen years of trials for their control with chemicals and biocontrol agents. *Plant Dis.* **2018**, *102*, 1189–1217. [[CrossRef](#)] [[PubMed](#)]
2. Wagschal, I.; Abou-Mansour, E.; Petit, A.-N. Wood diseases of grapevine: A review on eutypa dieback and esca. In *Plant-Microbe Interactions*; Ait Barka, E., Clément, C., Eds.; Research Signpost: Trivandrum, India, 2008; pp. 1–25.
3. Bertsch, C.; Ramírez-Suero, M.; Magnin-Robert, M.; Larignon, P.; Chong, J.; Abou-Mansour, E.; Spagnolo, A.; Clément, C.; Fontaine, F. Grapevine trunk diseases: Complex and still poorly understood. *Plant Pathol.* **2013**, *62*, 243–265. [[CrossRef](#)]
4. Gramaje, D.; Úrbez-Torres, J.R.; Sosnowski, M.R. Managing grapevine trunk diseases with respect to etiology and epidemiology: Current strategies and future prospects. *Plant Dis.* **2018**, *102*, 12–39. [[CrossRef](#)] [[PubMed](#)]
5. Hofstetter, V.; Buyck, B.; Croll, D.; Viret, O.; Couloux, A.; Gindro, K. What if esca disease of grapevine were not a fungal disease? *Fungal Divers.* **2012**, *54*, 51–67. [[CrossRef](#)]
6. Broda, M. Natural Compounds for Wood Protection against Fungi—A Review. *Molecules* **2020**, *25*, 3538. [[CrossRef](#)]
7. Yiamsawas, D.; Beckers, S.J.; Lu, H.; Landfester, K.; Wurm, F.R. Morphology-controlled synthesis of lignin nanocarriers for drug delivery and carbon materials. *ACS Biomater. Sci. Eng.* **2017**, *3*, 2375–2383. [[CrossRef](#)]
8. Yiamsawas, D.; Baier, G.; Thines, E.; Landfester, K.; Wurm, F.R. Biodegradable lignin nanocontainers. *RSC Adv.* **2014**, *4*, 11661–11663. [[CrossRef](#)]
9. Fischer, J.; Beckers, S.J.; Yiamsawas, D.; Thines, E.; Landfester, K.; Wurm, F.R. Targeted drug delivery in plants: Enzyme-responsive lignin nanocarriers for the curative treatment of the worldwide grapevine trunk disease Esca. *Adv. Sci.* **2019**, *6*, 1802315. [[CrossRef](#)]
10. Wurm, F.R.; Weiss, C.K. Nanoparticles from renewable polymers. *Front. Chem.* **2014**, *2*, 49. [[CrossRef](#)]
11. Pathania, D.; Gupta, D.; Agarwal, S.; Asif, M.; Gupta, V.K. Fabrication of chitosan-g-poly(acrylamide)/CuS nanocomposite for controlled drug delivery and antibacterial activity. *Mater. Sci. Eng. C* **2016**, *64*, 428–435. [[CrossRef](#)]
12. Beckers, S.J.; Wetherbee, L.; Fischer, J.; Wurm, F.R. Fungicide-loaded and biodegradable xylan-based nanocarriers. *Biopolymers* **2020**, *111*, e23413. [[CrossRef](#)] [[PubMed](#)]
13. Ciftci, N.; Sargin, I.; Arslan, G.; Arslan, U.; Okudan, A. Ascorbic acid adsorption-release performance and antibacterial activity of chitosan-ter(GMA-MA-NTBA) polymer microcapsules. *J. Polym. Environ.* **2020**, *28*, 2277–2288. [[CrossRef](#)]
14. Zou, T.; Sipponen, M.H.; Österberg, M. Natural shape-retaining microcapsules with shells made of chitosan-coated colloidal lignin particles. *Front. Chem.* **2019**, *7*, 370. [[CrossRef](#)] [[PubMed](#)]
15. Rosova, E.; Smirnova, N.; Dresvyanina, E.; Smirnova, V.; Vlasova, E.; Ivan’kova, E.; Sokolova, M.; Maslennikova, T.; Malafeev, K.; Kolbe, K.; et al. Biocomposite materials based on chitosan and lignin: Preparation and characterization. *Cosmetics* **2021**, *8*, 24. [[CrossRef](#)]
16. Aradmehr, A.; Javanbakht, V. A novel biofilm based on lignocellulosic compounds and chitosan modified with silver nanoparticles with multifunctional properties: Synthesis and characterization. *Colloids Surf. A Physicochem. Eng. Asp.* **2020**, *600*, 124952. [[CrossRef](#)]
17. Machado, T.O.; Beckers, S.J.; Fischer, J.; Müller, B.; Sayer, C.; de Araújo, P.H.H.; Landfester, K.; Wurm, F.R. Bio-based lignin nanocarriers loaded with fungicides as a versatile platform for drug delivery in plants. *Biomacromolecules* **2020**, *21*, 2755–2763. [[CrossRef](#)]
18. Peil, S.; Beckers, S.J.; Fischer, J.; Wurm, F.R. Biodegradable, lignin-based encapsulation enables delivery of *Trichoderma reesei* with programmed enzymatic release against grapevine trunk diseases. *Mater. Today Bio* **2020**, *7*, 100061. [[CrossRef](#)]
19. Langa-Lomba, N.; Buzón-Durán, L.; Martín-Ramos, P.; Casanova-Gascón, J.; Martín-Gil, J.; Sánchez-Hernández, E.; González-García, V. Assessment of conjugate complexes of chitosan and *Urtica dioica* or *Equisetum arvense* extracts for the control of grapevine trunk pathogens. *Agronomy* **2021**, *11*, 976. [[CrossRef](#)]

20. Langa-Lomba, N.; Sánchez-Hernández, E.; Buzón-Durán, L.; González-García, V.; Casanova-Gascón, J.; Martín-Gil, J.; Martín-Ramos, P. Activity of anthracenediones and flavoring phenols in hydromethanolic extracts of *Rubia tinctorum* against grapevine phytopathogenic fungi. *Plants* **2021**, *10*, 1527. [[CrossRef](#)]
21. Langa-Lomba, N.; Buzón-Durán, L.; Sánchez-Hernández, E.; Martín-Ramos, P.; Casanova-Gascón, J.; Martín-Gil, J.; González-García, V. Antifungal activity against Botryosphaeriaceae fungi of the hydro-methanolic extract of *Silybum marianum* capitula conjugated with stevioside. *Plants* **2021**, *10*, 1363. [[CrossRef](#)]
22. Leonardo, D.-C. Botryosphaeriaceae species associated with stem canker, die-back and fruit rot on apple in Uruguay. *Eur. J. Plant Pathol.* **2016**, *146*, 637–655. [[CrossRef](#)]
23. Szegedi, E.; Civerolo, E.L. Bacterial diseases of grapevine. *Int. J. Hortic. Sci.* **2011**, *17*, 45–49. [[CrossRef](#)]
24. Stevens, N.E. Two apple black rot fungi in the United States. *Mycologia* **2018**, *25*, 536–548. [[CrossRef](#)]
25. Brown-Rytlewski, D.E.; McManus, P.S. Virulence of *Botryosphaeria dothidea* and *Botryosphaeria obtusa* on apple and management of stem cankers with fungicides. *Plant Dis.* **2000**, *84*, 1031–1037. [[CrossRef](#)] [[PubMed](#)]
26. Willems, A.; Gillis, M.; Kersters, K.; Van Den Broecke, L.; De Ley, J. Transfer of *Xanthomonas ampelina* Panagopoulos 1969 to a new genus, *Xylophilus* gen. nov., as *Xylophilus ampelinus* (Panagopoulos 1969) comb. nov. *Int. J. Syst. Bacteriol.* **1987**, *37*, 422–430. [[CrossRef](#)]
27. Gerin, D.; Cariddi, C.; de Miccolis Angelini, R.M.; Rotolo, C.; Dongiovanni, C.; Faretra, F.; Pollastro, S. First report of *Pseudomonas* grapevine bunch rot caused by *Pseudomonas syringae* pv. *syringae*. *Plant Dis.* **2019**, *103*, 1954–1960. [[CrossRef](#)]
28. Santos-Moriano, P.; Fernandez-Arrojo, L.; Mengibar, M.; Belmonte-Reche, E.; Peñalver, P.; Acosta, F.N.; Ballesteros, A.O.; Morales, J.C.; Kidibule, P.; Fernandez-Lobato, M.; et al. Enzymatic production of fully deacetylated chitoooligosaccharides and their neuroprotective and anti-inflammatory properties. *Biocatal. Biotransform.* **2017**, *36*, 57–67. [[CrossRef](#)]
29. Buzón-Durán, L.; Martín-Gil, J.; Pérez-Lebeña, E.; Ruano-Rosa, D.; Revuelta, J.L.; Casanova-Gascón, J.; Ramos-Sánchez, M.C.; Martín-Ramos, P. Antifungal agents based on chitosan oligomers, ϵ -polylysine and *Streptomyces* spp. secondary metabolites against three Botryosphaeriaceae species. *Antibiotics* **2019**, *8*, 99. [[CrossRef](#)]
30. Sannan, T.; Kurita, K.; Iwakura, Y. Studies on chitin, 2. Effect of deacetylation on solubility. *Makromol. Chem.* **1976**, *177*, 3589–3600. [[CrossRef](#)]
31. Yang, Y.; Shu, R.; Shao, J.; Xu, G.; Gu, X. Radical scavenging activity of chitoooligosaccharide with different molecular weights. *Eur. Food Res. Technol.* **2005**, *222*, 36–40. [[CrossRef](#)]
32. Maghami, G.G.; Roberts, G.A.F. Evaluation of the viscometric constants for chitosan. *Makromol. Chem.* **1988**, *189*, 195–200. [[CrossRef](#)]
33. Tian, M.; Tan, H.; Li, H.; You, C. Molecular weight dependence of structure and properties of chitosan oligomers. *RSC Adv.* **2015**, *5*, 69445–69452. [[CrossRef](#)]
34. Krizsán, K.; Szókán, G.; Toth, Z.A.; Hollósy, F.; László, M.; Khlafulla, A. HPLC analysis of anthraquinone derivatives in madder root (*Rubia tinctorum*) and its cell cultures. *J. Liq. Chromatogr. Relat. Technol.* **2006**, *19*, 2295–2314. [[CrossRef](#)]
35. Cruz, G.; Crnkovic, P.M. Investigation into the kinetic behavior of biomass combustion under N₂/O₂ and CO₂/O₂ atmospheres. *J. Therm. Anal. Calorim.* **2015**, *123*, 1003–1011. [[CrossRef](#)]
36. Arendrup, M.C.; Cuenca-Estrella, M.; Lass-Flörl, C.; Hope, W. EUCAST technical note on the EUCAST definitive document EDef 7.2: Method for the determination of broth dilution minimum inhibitory concentrations of antifungal agents for yeasts EDef 7.2 (EUCAST-AFST). *Clin. Microbiol. Infect.* **2012**, *18*, E246–E247. [[CrossRef](#)]
37. CLSI. *Methods for Dilution Antimicrobial Susceptibility Tests for Bacteria That Grow Aerobically*, 11th ed.; CLSI standard M07; Clinical and Laboratory Standards Institute: Wayne, PA, USA, 2018.
38. Choudhary, R.C.; Kumari, S.; Kumaraswamy, R.V.; Pal, A.; Raliya, R.; Biswas, P.; Saharan, V. Characterization methods for chitosan-based nanomaterials. In *Plant Nanobionics*; Springer: Cham, Switzerland, 2019; pp. 103–116. [[CrossRef](#)]
39. Kumaraswamy, R.V.; Kumari, S.; Choudhary, R.C.; Pal, A.; Raliya, R.; Biswas, P.; Saharan, V. Engineered chitosan based nanomaterials: Bioactivities, mechanisms and perspectives in plant protection and growth. *Int. J. Biol. Macromol.* **2018**, *113*, 494–506. [[CrossRef](#)]
40. Bhattacharjee, S. DLS and zeta potential—What they are and what they are not? *J. Controll. Release* **2016**, *235*, 337–351. [[CrossRef](#)]
41. Machado, T.O.; Beckers, S.J.; Fischer, J.; Sayer, C.; de Araújo, P.H.H.; Landfester, K.; Wurm, F.R. Cellulose nanocarriers via miniemulsion allow pathogen-specific agrochemical delivery. *J. Colloid Interface Sci.* **2021**, *601*, 678–688. [[CrossRef](#)]
42. Wurm, F.; Landfester, K.; Yiamsawas, D.; Thines, E.; Fischer, J. Lignin Biomaterial as Agricultural Drug Carrier. U.S. Patent 2019/0037837 A1, 7 February 2019.
43. Tang, G.; Tian, Y.; Niu, J.; Tang, J.; Yang, J.; Gao, Y.; Chen, X.; Li, X.; Wang, H.; Cao, Y. Development of carrier-free self-assembled nanoparticles based on fenhexamid and polyhexamethylene biguanide for sustainable plant disease management. *Green Chem.* **2021**, *23*, 2531–2540. [[CrossRef](#)]